

新疆包古图斑岩铜矿 III-2 岩体氧逸度研究： 来自矿物成分的指示

魏少妮¹⁾，朱永峰²⁾，安芳³⁾

1) 西安科技大学地质与环境学院，西安，710054；

2) 北京大学地球与空间科学学院，北京，100871；3) 西北大学地质系，西安，710069

内容提要：包古图斑岩铜矿位于新疆西准噶尔地区，是区内规模最大的斑岩型矿床，成矿作用与晚石炭世中酸性侵入体密切相关。III-2 岩体位于矿区南部，该岩体全岩矿化，但品位较低，是探讨成矿岩浆性质的理想对象。本文结合岩石学和角闪石、锆石等矿物成分分析，通过与典型斑岩铜矿进行对比，探讨了成矿岩浆的氧逸度。研究表明，包古图 III-2 岩体以石英闪长(玢)岩和闪长岩为主，少量辉石闪长岩，主要由斜长石、角闪石、黑云母、石英和钾长石组成，含少量钛铁矿、榍石和磷灰石。石英闪长岩中早期结晶的自形角闪石属于钙质闪石， $Mg^{\#}$ 较高(0.72~1.00)，成分分析指示成矿岩浆的氧逸度为： $\Delta NNO+1.4\sim\Delta NNO+2.6$ ，位于斑岩铜矿含矿岩体的分布范围。从中分选出的锆石 REE 含量高($338\times 10^{-6}\sim 959\times 10^{-6}$)，具有左倾型稀土配分模式，轻稀土亏损，重稀土富集，显示强烈 Ce 正异常和 Eu 负异常。 Ce^{4+}/Ce^{3+} 比值为 29.55~89.50， Eu/Eu^* 比值为 0.32~0.47，分布于斑岩铜矿含矿岩体和未矿化岩体的叠加部位。研究结果显示，包古图斑岩铜矿 III-2 岩体成矿岩浆氧逸度较高，有利于成矿元素的溶解和迁移，对斑岩铜矿的形成有促进作用。

关键词：氧逸度；斑岩铜矿；成矿岩浆；包古图；西准噶尔

斑岩型矿床提供了全世界 70% 的 Cu，50% 的 Mo 以及 25% 的 Au (Sillitoe, 2010)。这类矿床的形成经历了从岩浆到热液的演化过程，成矿岩浆的氧逸度是制约斑岩成矿作用的关键因素之一 (Richards, 2005; Sun Weidong et al., 2015; Williamson et al., 2016; Hattori, 2018)。世界上绝大多数的斑岩矿床都具有高氧逸度的成矿岩浆，在 Ni-NiO(NNO) 氧逸度缓冲对和磁铁矿-赤铁矿 (HM) 氧逸度缓冲对之间，通常 $\log f_{O_2} > FMQ + 2$ (Mungall, 2002; Richards, 2003; FMQ 为铁橄榄石-磁铁矿-石英氧逸度缓冲对)。部分矿床可见岩浆成因的硬石膏 (Stern et al., 2007; Chambefort et al., 2008)，指示成矿体系高的氧逸度和硫含量。少数还原型斑岩矿床成矿岩浆氧逸度较低 ($\log f_{O_2} < FMQ$, Rowins, 2000; Smith et al., 2012)，含有岩浆成因硫化物(如磁黄铁矿)，未见硬石膏、赤铁矿

等高氧化态矿物。与氧化型斑岩矿床相比，还原型斑岩矿床数量少、储量低。Richards (2005) 指出，高水含量、高氧逸度的岩浆，是产出巨型斑岩矿床的首要因素。Wang Rui et al. (2017) 研究认为藏南侏罗纪冈底斯岛弧中超大型斑岩 Cu-Au 矿的形成与岛弧前缘富水、高氧逸度的岩浆有关。Bao Xinshang et al. (2018) 指出成矿岩浆高的氧逸度和水含量是形成云南北衙巨型斑岩 Au 矿的制约因素。

新疆西准噶尔包古图地区发育多个矿化侵入体 (I~V)，不同岩体蚀变矿化程度差别明显。其中 V 号岩体矿化强烈，产出斑岩型铜矿体，已探明 Cu 金属量 64Mt (平均品位 0.28%)，伴生 Mo 1.8Mt，Au 14t，Ag 377t (Zhang Rui et al., 2006)。关于包古图地区的斑岩型铜矿化作用，前人已做了大量工作，在矿床地质、成矿流体、成岩成矿时代等方面积累了

注：本文为国家自然科学基金项目 (No. 41403033; No. 41602212) 和陕西省自然科学基金基础研究计划一般项目 (面上) (2019JM-409) 联合资助成果。

收稿日期：2019-07-28；改回日期：2019-11-01；网络发表日期：2019-12-31；责任编辑：范宏瑞；责任编辑：黄敏。

作者简介：魏少妮，女，1984 年生。副教授，硕士生导师，主要从事矿床地球化学研究。Email: weishaoni03@163.com。

引用本文：魏少妮，朱永峰，安芳. 2020. 新疆包古图斑岩铜矿 III-2 岩体氧逸度研究：来自矿物成分的指示. 地质学报, 94(8): 2367~2382, doi: 10.19762/j.cnki.dizhixuebao.2020042.
Wei Shaoni, Zhu Yongfeng, An Fang. 2020. Oxygen fugacity of the intrusion III-2 in the Baogutu porphyry copper deposit, Xinjiang: evidence from mineral compositions. Acta Geologica Sinica, 94(8): 2367~2382.

大量研究成果 (Zhang Lianchang et al., 2006; Song Huixia et al., 2007; Shen Ping et al., 2012, 2015a; Wei Shaoni et al., 2015; Cao Mingjian et al., 2014, 2017), 但是关于成矿岩浆的氧化-还原特征仍然存在争议。Cao Mingjian et al. (2014) 指出包古图斑岩铜矿具有“还原型”斑岩铜矿床的特征, 成矿岩浆氧逸度较低 $\log f_{O_2} = \Delta NNO$ 。Shen Ping et al. (2015a) 通过含矿闪长岩的黑云母、角闪石成分和磷灰石的 SO_3 含量认为成矿岩浆的氧逸度为 $\log f_{O_2} > \Delta FMQ + 1$ (FMQ 为铁橄榄石-磁铁矿-石英氧逸度缓冲对)。Cao Mingjian et al. (2017) 给出了两个完全不同的氧逸度值: 锆石 Ce 含量指示成矿岩浆的氧逸度 $\log f_{O_2} = \Delta NNO + 0.6$, 黑云母 Fe^{2+} 、 Fe^{3+} 含量指示 $\log f_{O_2} < \Delta NNO$ (NNO 为 Ni-NiO 氧逸度缓冲对)。Zhu Bin et al. (2018) 认为有两个岩浆阶段, 早期氧化阶段形成磁铁矿和高 $Mg^{\#}$ 角闪石 ($\log f_{O_2} > \Delta NNO + 2.4$), 晚期还原阶段形成钛铁矿和低 $Mg^{\#}$ 黑云母 ($\log f_{O_2} < \Delta NNO - 0.6$), 并认为后期氧逸度的降低与有机碳的还原作用有关。Wei Shaoni et al. (2019) 结合锆石 Ce^{4+}/Ce^{3+} 比值、角闪石、黑云母成分特征和全岩 Fe^{3+}/Fe^{2+} 比值获得成矿岩浆的氧逸度为 $\Delta FMQ + 2.5 \sim \Delta FMQ + 2.7$ 。包古图 III-2 岩体位于矿区南部, 该岩体全岩矿化但整体品位较低, 是探讨成矿岩浆相关特征的理想对象。本文以 III-2 岩体为研究对象, 在前人研究的基础上, 通过角闪石、锆石等矿物成分分析, 探讨成矿岩浆的氧逸度及其成矿制约, 为斑岩体系成矿作用的完善提供资料。

1 区域地质

新疆西准噶尔地区是中亚成矿域的重要组成部分, 位于巴尔喀什-准噶尔地体的东端 (Zhu Yongfeng et al., 2013, 2016)。西准地区分布多条蛇绿岩带, 玛依勒蛇绿混杂岩形成于早-中寒武世, 为 SSZ 型蛇绿混杂岩 (Ren Rong et al., 2014)。塔尔巴哈台-库吉拜-洪古勒楞蛇绿混杂岩带和唐巴勒-白碱滩-百口泉蛇绿混杂岩带形成于奥陶纪, 代表了古洋壳残片 (Zhu Yongfeng et al., 2015)。达拉布特-萨尔托海蛇绿混杂岩带自中志留世持续至早泥盆世, 是西准地区最年轻的蛇绿岩带 (Chen Bo et al., 2011; Yang Gaoxue et al., 2012; Zhu Yongfeng et al., 2013)。泥盆纪砾岩-砂岩和早石炭世火山-沉积岩不整合覆盖在蛇绿岩及其相关复理石建造之上。下石炭统火山沉积地层是西准噶尔

地区的主要盖层, 包括希贝库拉斯组、包古图组和太勒古拉组 (图 1)。希贝库拉斯组主要由含砾砂岩和凝灰质粉砂岩组成。包古图组主要为凝灰质粉砂岩和凝灰岩, 凝灰岩的锆石 U-Pb 年龄为 328~342Ma (An Fang et al., 2009)。太勒古拉组由粉砂岩、凝灰岩和中-基性火山岩组成, 凝灰岩的锆石 U-Pb 年龄为 328Ma (Wang Rui et al., 2007)。

西准噶尔地区广泛发育晚古生代侵入岩 (图 1), 大型花岗质岩基侵位于蛇绿混杂岩和下石炭统火山-沉积地层之中, 侵位时间集中在 290~310Ma (Han Baofu et al., 2006; Zhu Yongfeng et al., 2013; Duan Fenghao et al., 2018)。闪长质到花岗质岩株和岩脉侵位于下石炭统火山-沉积地层中, 集中分布在包古图区域, 侵位时间为 310~320Ma (Liu Yulin et al., 2009; Shen Ping et al., 2012; Wei Shaoni et al., 2015)。辉长质到闪长质岩墙侵位于火山-沉积地层和花岗质岩基之中, 侵位时间集中在 240~280Ma (Li Xinzi et al., 2004; Yin Jiyuan et al., 2013)。这些侵入岩均显示高的 $\epsilon_{Nd}(t)$ 值 (Han Baofu et al., 1997; Gao Rui et al., 2014), 部分岩石显示出埃达克岩的特征, 被认为是洋脊俯冲的产物 (Geng Hongyan et al., 2009; Tang Gongjian et al., 2012), 但也有观点认为这些侵入岩形成于洋内俯冲 (Xu Yixian et al., 2016; Zhang Jien et al., 2011) 或后碰撞环境 (Han Baofu et al., 2006; Zhu Yongfeng et al., 2013; Zhang Huichao et al., 2018)。

西准噶尔地区矿产资源丰富, 以 NE 走向的达拉布特断裂为界, 哈图-萨尔托海矿集区分布于断裂以北, 产出哈图金矿、宝贝金矿、辉绿山金矿、满喇山金矿、萨尔托海铬铁矿等众多矿床 (图 1); 包古图矿集区位于达拉布特断裂以南, 产出包古图金矿、包古图斑岩铜矿和宏远钼矿 (图 1, 图 2a)。包古图斑岩铜矿是西准地区唯一的大型铜矿床, 并伴生产出钼和金。铜矿体赋存于矿化岩体及其邻近的蚀变围岩中, 浅部主要是浸染状矿化, 深部为浸染状和细脉-网脉状矿化。热液蚀变和矿化具有明显的分带性, 从内向外依次发育 Ca-Na 硅酸盐蚀变带、钾质蚀变带、绢云母化带和青磐岩化带 (Shen Ping et al., 2009; Wei Shaoni, 2012)。此外, 在岩体与围岩接触带发育金矿化 (Zheng Bo et al., 2015) 和少量铋矿化 (Wei Shaoni et al., 2017)。辉钼矿 Re-Os 同位素指示成矿时代为 310~312Ma (Song Huixia et al., 2007; Shen Ping et al., 2012)。

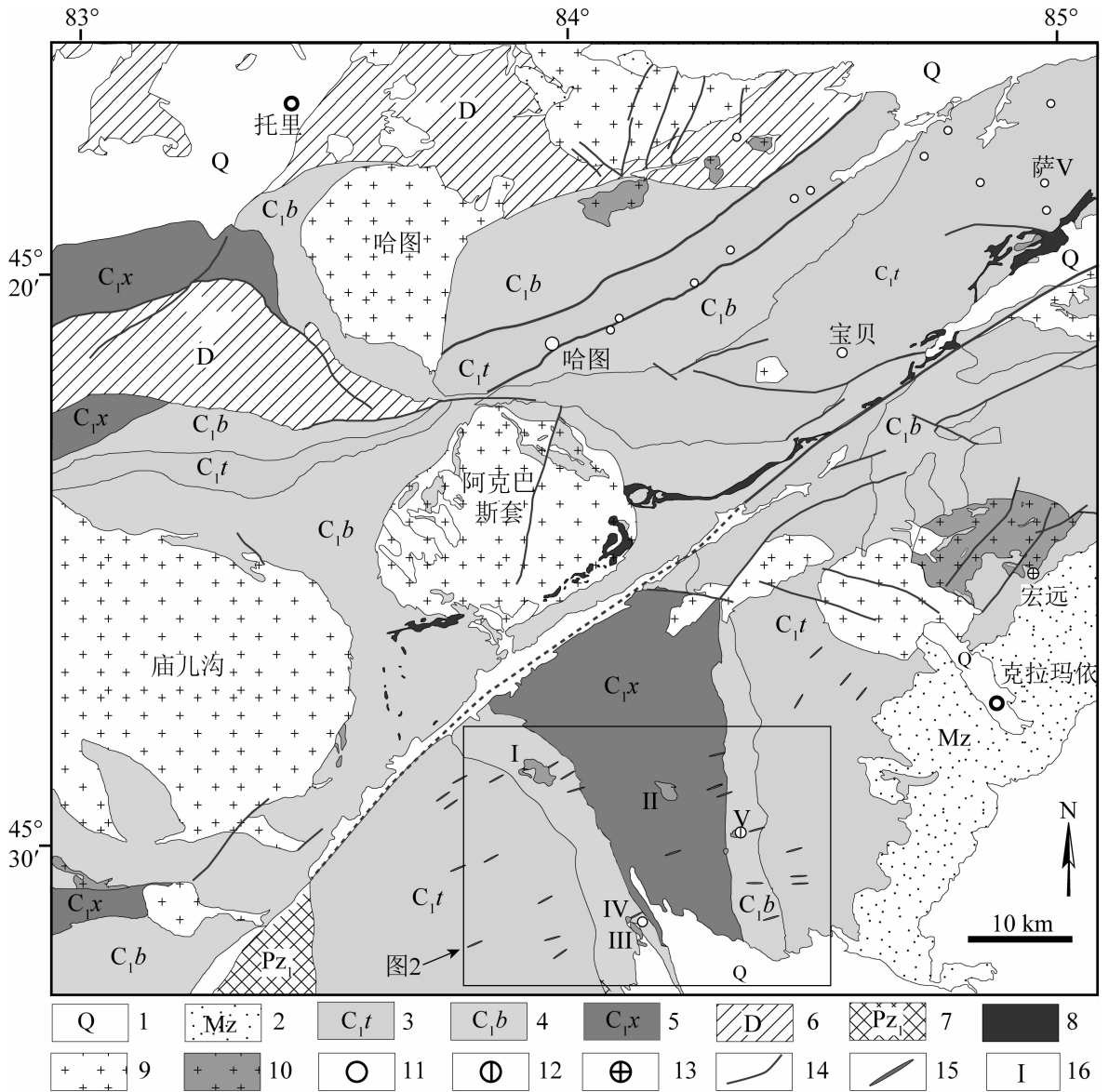


图 1 西准噶尔地质简图(据新疆维吾尔自治区地质矿产局, 1993)

Fig. 1 Simplified geological map of the west Junggar (modified after BGMRX, 1993)

1—第四系; 2—中生界地层; 3—下石炭统太勒古拉组; 4—下石炭统包古图组; 5—下石炭统希贝库拉斯组; 6—泥盆系地层; 7—下古生界地层; 8—超基性岩; 9—花岗岩; 10—花岗闪长岩; 11—金矿点; 12—铜矿; 13—钼矿; 14—断裂; 15—脉岩; 16—岩体编号

1—Quaternary; 2—Mesozoic Formation; 3—Tailegula Formation of Lower Carboniferous; 4—Baogutu Formation of Early Carboniferous; 5—Xibeikulasi Formation of Early Carboniferous; 6—Devonian Formation; 7—Lower Palaeozoic Formation; 8—ultramafic unit; 9—granite; 10—granodiorite; 11—gold occurrence; 12—copper deposit; 13—molybdenum deposit; 14—fault; 15—dyke; 16—intrusion number

2 矿区地质

包古图斑岩铜矿是西准噶尔地区规模最大的斑岩型矿床, 矿区范围内出露多个矿化岩体, I 号岩体邻近达拉布特断裂分布, 侵位于包古图组中。II 号岩体呈菱形展布, 出露于包古图地区中部, 侵位于希贝库拉斯组中。III 号岩体为 NW-SE 向展布的椭圆形, 出露面积 1.76km², 位于包古图地区南部。IV 号岩体位于 III 号岩体北侧, 二者均侵位于包古

图组中。V 号岩体出露面积 0.84km², 呈不规则钟状, 位于包古图地区东部, 东侧出露包古图组, 西侧出露太勒古拉组(图 2a)。各岩体蚀变矿化差异明显, I、II、IV 号岩体矿化较差, 仅发育少量浸染状黄铜矿和黄铁矿。V 号岩体矿化强烈, 发育浸染状、脉状和角砾状 Cu-Mo-Au 矿化, 矿体赋存于岩体及其与围岩接触带中。III 号岩体全岩矿化, 硫化物以浸染状(少数脉状)分布于岩体及其邻近围岩中, 但整体品位很低, 铜最高品位 0.94%, 金最高品位

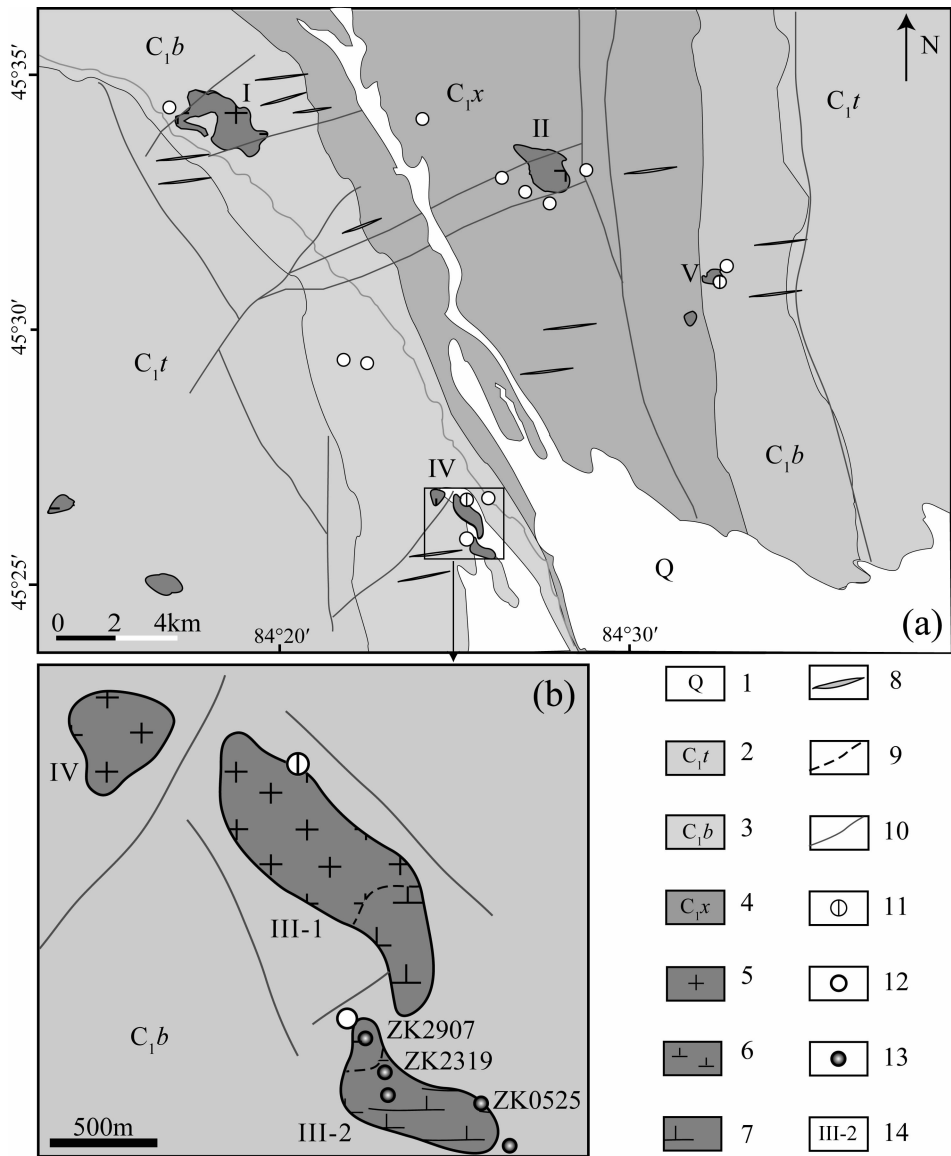


图 2 (a)—新疆包古图地区区域地质简图(修改自 Zheng Bo et al., 2015);

(b)—III 号岩体地质简图(据武警黄金第八支队内部资料绘制)

Fig. 2 (a)—Geological map of the Baogutu region, Xinjiang (modified after Zheng Bo et al., 2015);

(b)—simplified geological map of the intrusion III

(modified from internal data of No. 8 Gold Geological Party of Chinese People's Armed Police Force)

1—第四系; 2—太勒古拉组; 3—包古图组; 4—希贝库拉斯组; 5—花岗闪长岩; 6—石英闪长岩;

7—闪长岩; 8—岩墙; 9—相变界线; 10—断层; 11—铜矿; 12—金矿; 13—钻孔; 14—岩体编号

1—Quaternary; 2—Tailegula Formation; 3—Baogutu Formation; 4—Xibeikulasi Formation; 5—granodiorite; 6—quartz diorite;

7—diorite; 8—dyke; 9—face transition limit; 10—fault; 11—copper deposit; 12—gold deposit; 13—drill hole; 14—intrusion number

4.65g/t, 绝大多数样品低于边界品位。根据野外地质工作, 将 III 号岩体划分为北侧的 III-1 和南侧的 III-2 两部分, 本次研究的样品采自南侧 III-2 岩体。

3 岩石学特征

包古图 III-2 岩体共施工钻孔 5 个, 其中 4 个位于岩体内部, 1 个位于岩体南东侧包古图组地层中

(图 2b), 我们挑选其中三个进行了样品采集(图 3)。

ZK2907 位于 III-2 岩体北部, 终孔深度 300m, 显示岩体岩性为石英闪长岩, 局部岩芯段暗色矿物含量变化大, 过渡为黑云母石英闪长岩或角闪石英闪长岩。钻孔中见安山岩, 斑晶为斜长石和角闪石, 气孔发育, 被绿泥石和方解石充填。ZK2319 位于 III-2 岩体东侧, 终孔深度 918.45m, 分布在岩体边

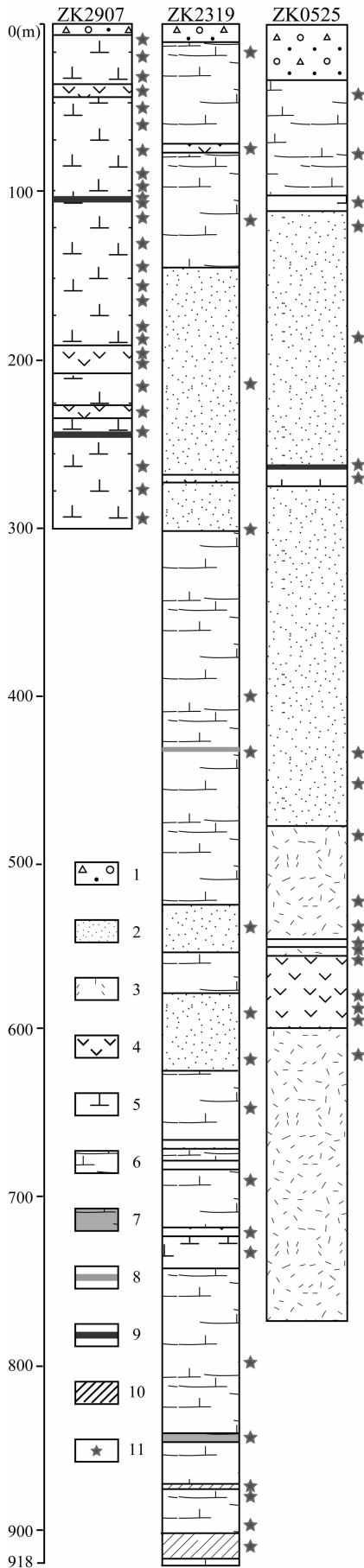


图 3 新疆包古图 III-2 岩体钻孔剖面图

Fig. 3 Section of drills in the Baogutu intrusion III-2, Xinjiang

1—第四系; 2—砂岩; 3—凝灰岩; 4—安山岩; 5—石英闪长岩; 6—闪长岩; 7—辉石闪长岩; 8—石英脉; 9—方解石-石英脉; 10—构造破碎带; 11—采样位置

1—Quaternary; 2—sandstone; 3—tuff; 4—andesite; 5—quartz diorite; 6—diorite; 7—pyroxene diorite; 8—quartz vein; 9—calcicite-quartz vein; 10—tectonic fracture zone; 11—sample location

部,岩芯中岩体和地层交替出现。岩体岩性以闪长岩为主,少量石英闪长岩和辉石闪长岩,地层岩性包括安山岩、石英砂岩和长石石英砂岩。钻孔深度 873.6m 和终孔的位置发育角砾岩,角砾为闪长岩,胶结物为石英和浊沸石。ZK0525 位于 III-2 岩体东侧边界,终孔深度 772.95m,岩芯顶部见少量岩体,中部和下部均为下石炭统火山沉积地层。岩体岩性为闪长岩和石英闪长岩,地层岩性为石英砂岩、凝灰岩和安山岩。

地表和钻孔样品显示,III-2 岩体岩性以石英闪长(玢)岩和闪长岩为主,少量辉石闪长岩,主要由斜长石、角闪石、黑云母、石英和钾长石组成,局部位置发育单斜辉石,含少量钛铁矿、榍石和磷灰石(图 4)。斜长石(50%~65%)呈自形板状,聚片双晶发育,部分颗粒显示环带结构,结晶较早;角闪石(10%~20%)浅黄-浅绿多色性,自形、半自形,与斜长石共生产出(图 4a);黑云母(5%~10%)浅黄-棕褐多色性,粒度细小,半自形到自形,与斜长石和角闪石共生产出,结晶较晚(图 4b);钾长石(5%~10%)和石英(5%~20%)呈它形粒状,充填颗粒间隙;单斜辉石(<5%)仅出现在部分钻孔样品中,沿边部和裂隙被角闪石交代(图 4c)。石英闪长玢岩断续出现,斜长石和角闪石是主要的斑晶相,约占总体积的 5%~15%,基质由粒度细小的板条状斜长石搭成格架,角闪石、黑云母和石英充填其中(图 4d)。

4 测试方法

矿物电子探针分析工作在中国科学院地质与地球物理研究所电子探针与电镜实验室进行,使用仪器为 JXA-8100,测试条件为:加速电压 15kV、束流 2×10^{-8} A,束斑 $5 \mu\text{m}$,修正方法 PRZ,使用的标样为美国 SPI 公司 53 种矿物,最低检出限 $\sim 0.01\%$ 。

锆石微量元素分析在西北大学大陆动力学国家重点实验室采用激光剥蚀-电感耦合等离子质谱分

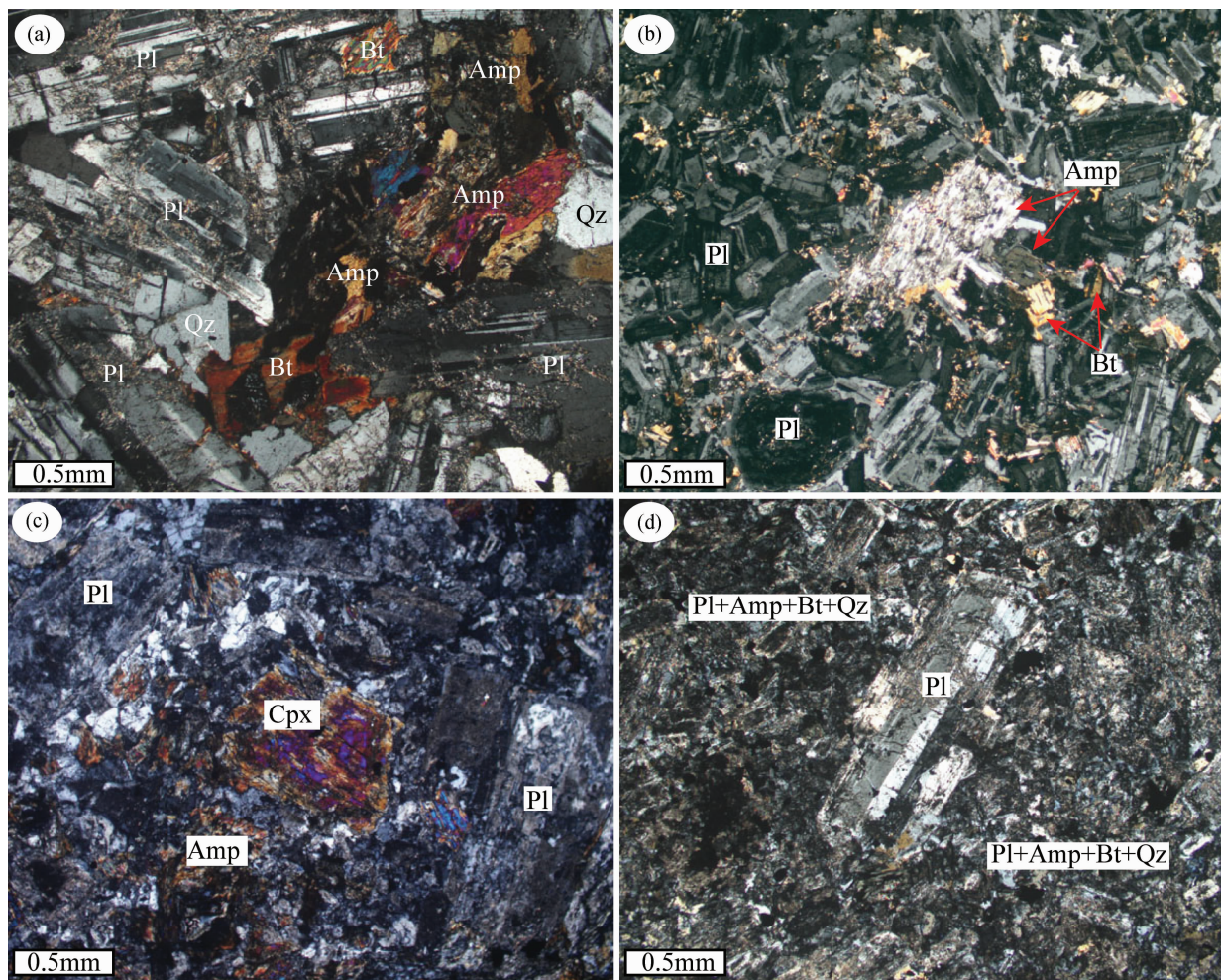


图4 新疆包古图 III-2 岩体显微岩相学照片

Fig. 4 Microphotographs of the Baogutu intrusion III-2, Xinjiang

(a)—石英闪长岩中的板状斜长石和自形角闪石,正交光;(b)—闪长岩显微特征,自形斜长石、角闪石结晶较早,它形-半自形黑云母结晶较晚,正交光;(c)—辉石闪长岩显微特征,辉石沿边部蚀变为角闪石,正交光;(d)—闪长玢岩中的斜长石斑晶,正交光;Pl—斜长石;Qz—石英;Bt—黑云母;Amp—角闪石;Cpx—单斜辉石

(a)—Quartz diorite with tabular plagioclase and euhedral amphibole, cross-polarized light; (b)—diorite with early stage enehedral plagioclase and amphibole, late stage unehedral-subhedral biotite, cross-polarized light; (c)—pyroxene diorite with clinopyroxene replaced by amphibole, cross-polarized light; (d)—diorite porphyry with plagioclase phenocrysts, cross-polarized light; Pl—plagioclase; Qz—quartz; Bt—biotite; Amp—amphibole; Cpx—clinopyroxene

析(LA-ICPMS)。激光剥蚀系统为德国 MicroLas 公司生产的 GeoLas200M, ICP-MS 为美国 Agilent 公司生产的 Agilent7500a。激光束斑直径为 $44\mu\text{m}$, 采样方式为单点剥蚀, 每个样品点的气体背景采集时间为 30s, 信号采集时间为 40s。数据处理采用 GLITTER(4.0)程序, 元素含量计算时以 NIST 610 为外标, Si 作内标。

5 测试结果

角闪石是包古图矿化侵入体中主要的造岩矿物, 呈自形-半自形产于岩体中。本次研究选取 III-2 岩体石英闪长岩中早期结晶的自形角闪石进

行电子探针分析, 所选矿物新鲜无蚀变。由测试结果可知(表 1), 包古图 III-2 岩体中的角闪石具有高的 MgO ($12.82\% \sim 16.59\%$)、 FeO ($12.24\% \sim 17.58\%$) 和 CaO ($9.71\% \sim 10.62\%$) 含量, K_2O ($0.22\% \sim 0.57\%$) 和 Na_2O ($0.77\% \sim 1.22\%$) 含量较低。属于钙质闪石, 成分投点位于镁质普通角闪石区域(图 5), $\text{Mg}^{\#}$ 较高($0.72 \sim 1.00$)。

从石英闪长岩中分选出的锆石颗粒形态规则, 以长柱状为主, 大小 $\sim 100\mu\text{m}$ 。阴极发光图像显示典型的扇形结构, 指示其岩浆成因(图 6a)。测试结果表明(表 2), 包古图 III-2 岩体中的锆石 REE 含量较高($338 \times 10^{-6} \sim 959 \times 10^{-6}$), Ti 含量变化范围为 8.17

表 1 新疆包古图 III-2 岩体角闪石电子探针分析结果 (%)

Table 1 Electron microprobe analysis results of amphibole from the Baogutu intrusion III-2, Xinjiang (%)

测点号	J341-1*	J341-2*	J341-3*	J341-4	J341-5	J341-6	J341-7	J341-8	J341-9	J341-10
SiO ₂	49.08	48.01	50.25	50.83	51.53	49.85	49.84	50.98	51.01	49.20
TiO ₂	1.10	1.17	0.62	0.66	0.27	0.86	0.44	0.37	0.43	0.62
Al ₂ O ₃	4.04	4.98	4.52	4.21	3.89	5.03	4.25	4.29	3.84	5.49
MgO	12.82	12.90	15.86	16.34	16.59	16.27	15.10	15.44	16.12	14.68
MnO	0.59	0.38	0.92	0.85	1.07	0.61	0.74	0.92	0.90	0.62
FeO	17.58	16.60	13.17	12.76	12.94	12.24	14.41	14.66	14.13	14.70
Cr ₂ O ₃	0	0	0	0.02	0	0.02	0	0.02	0	0.02
NiO	0	0.01	0	0	0.01	0	0	0.01	0.04	0.03
CaO	10.34	10.58	10.61	10.18	10.01	10.62	10.39	9.71	9.83	10.43
Na ₂ O	1.01	1.21	1.01	1.14	0.84	1.12	0.85	0.87	0.77	1.22
K ₂ O	0.40	0.57	0.33	0.27	0.23	0.40	0.30	0.30	0.22	0.43
F	0	0	0	0	0	0	0	0	0	0
Cl	0.17	0.23	0.15	0.11	0.10	0.14	0.14	0.15	0.11	0.18
总量	97.09	96.58	97.40	97.33	97.46	97.14	96.42	97.68	97.36	97.56
O=23										
Si(T)	7.171	7.077	7.141	7.179	7.220	7.086	7.170	7.173	7.170	7.039
Al ^{IV} (T)	0.695	0.865	0.757	0.700	0.643	0.843	0.720	0.712	0.635	0.925
Ti(T)	0.120	0.058	0.066	0.070	0.029	0.071	0.048	0.039	0.046	0.036
Al ^{VI} (C)	0	0	0	0	0	0	0	0	0	0
Ti(C)	0	0.072	0	0	0	0.021	0	0	0	0.030
Cr(C)	0	0	0	0.002	0	0.002	0	0.002	0	0.002
Fe ⁺³ (C)	1.126	0.927	1.261	1.358	1.584	1.185	1.350	1.642	1.727	1.250
Mg(C)	2.792	2.834	3.361	3.440	3.416	3.448	3.238	3.239	3.273	3.130
Fe ²⁺ (C)	1.022	1.119	0.304	0.149	0	0.270	0.383	0.083	0	0.508
Mn(C)	0.060	0.047	0.075	0.051	0	0.074	0.028	0.034	0	0.075
Ca(C)	0	0.002	0	0	0	0	0	0	0	0.004
Mg(B)	0	0	0	0	0.050	0	0	0	0.104	0
Mn(B)	0.014	0	0.036	0.051	0.126	0	0.062	0.075	0.107	0
Ca(B)	1.619	1.668	1.615	1.540	1.503	1.616	1.602	1.464	1.480	1.594
Na(B)	0.381	0.332	0.385	0.460	0.497	0.384	0.398	0.536	0.520	0.406
Na(A)	0	0.015	0	0	0	0	0	0	0	0
K(A)	0.074	0.108	0.060	0.049	0.042	0.073	0.056	0.054	0.039	0.078
Mg [#]	0.73	0.72	0.92	0.96	1.00	0.93	0.89	0.98	1.00	0.86
P(kbar)	0.30	1.11	0.60	0.32	0.05	1.00	0.42	0.38	0.01	1.39
logf _{O₂}	-12.07	-12.37	-10.95	-10.86	-10.92	-10.69	-11.30	-11.14	-10.73	-11.44
△NNO	1.6	1.4	2.3	2.5	2.6	2.4	2.2	2.3	2.6	1.9
T(°C)	810	803	826	824	814	836	815	818	827	820

注: $Mg^{\#} = Mg^{2+} / (Mg^{2+} + Fe^{2+})$; 角闪石结晶压力根据 Schmidt (1992) 公式计算; 角闪石结晶温度和氧逸度根据 Ridolfi et al., (2010) 公式计算。

$\times 10^{-6} \sim 28.72 \times 10^{-6}$, Th/U 比值 1.39~2.42。在球粒陨石标准化的稀土配分模式图上重稀土强烈富集, 具有明显的 Ce 正异常和 Eu 负异常(图 6b)。

6 讨论

6.1 成矿岩浆的氧逸度

6.1.1 角闪石成分氧逸度计

角闪石是钙碱性岩浆岩中最常见的造岩矿物, 其稳定性与岩浆体系的氧逸度、水含量和熔体成分有关(Sisson et al., 1993; Grove et al., 2003)。Anderson et al. (1995) 确定了不同氧逸度条件下,

角闪石 $Fe/(Fe+Mg)$ 值和 ^{IV}Al 的变化范围。在 $Fe/(Fe+Mg)^{-IV}Al$ 图解中(图 7a), 斑岩铜矿含矿和未矿化岩体均分布于高氧逸度区, 指示成矿作用与高氧逸度的岩浆有关。包古图 III-2 岩体石英闪长岩中的角闪石分布于含矿岩体的区域内, 说明包古图成矿岩浆具有较高的氧化状态。

Ridolfi et al., (2010) 通过实验研究给出了氧逸度与角闪石成分之间的关系式:

$$\Delta NNO = 1.644Mg^* - 4.01 \quad (R^2 = 0.89)$$

其中 $Mg^* = Mg + Si/47 - ^{VI}Al/9 - 1.3^{VI}Ti + Fe^{3+}/3.7 + Fe^{2+}/5.2 - ^B Ca/20 - ^A Na/2.8 + ^A [] /$

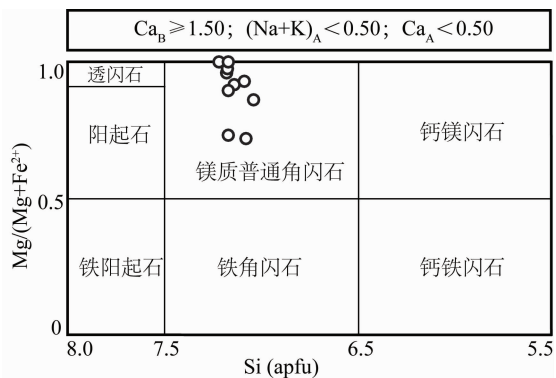


图5 新疆包古图 III-2 岩体石英闪长岩角闪石分类图解(底图据 Leake et al., 1997)

Fig. 5 Classification diagram of amphibole in quartz diorite from the Baogutu intrusion III-2, Xinjiang (after Leake et al., 1997)

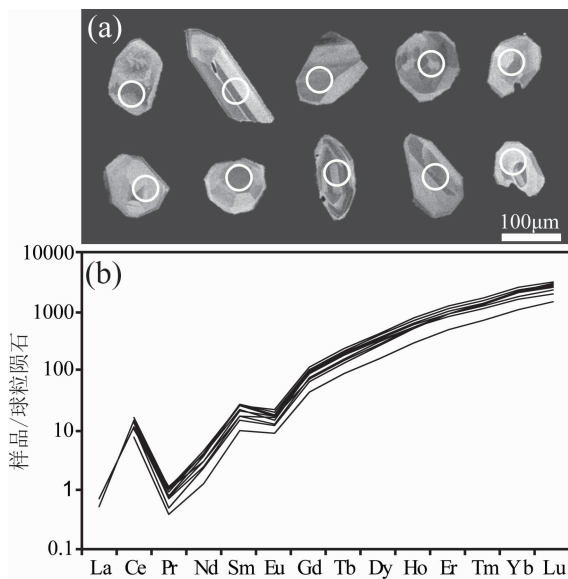


图6 新疆包古图 III-2 岩体锆石 CL 图像(a)和球粒陨石标准化稀土配分模式图(b) (标准化值据 Sun et al., 1989)

Fig. 6 Cathodoluminescence (CL) images (a) and chondrite-normalized REE patterns (b) for zircons from the Baogutu intrusion III-2, Xinjiang (normalization values are from Sun et al., 1989)

9.5, NNO 为 Ni-NiO 氧逸度缓冲对。公式计算误差为 $\pm 0.22 \log f_{O_2}$, 在实验预估误差范围内 ($0.2 \sim 0.3 \log f_{O_2}$, Scaillet et al., 1991; Pichavant et al., 2002)。该氧逸度计适用于温度 $500 \sim 1200^\circ\text{C}$, 压力 $< 1200 \text{ MPa}$, 氧逸度 $\Delta\text{NNO}-1$ 到 $\Delta\text{NNO}+5$ 之间的岩浆。Ayati et al. (2012) 用该方法计算获得 Dalli 斑岩铜-金矿含矿闪长玢岩和花岗闪长斑岩的氧逸度为 $\Delta\text{NNO}+1.3$ 。Li Jinxiang et al. (2018) 用该方法获得西藏多龙矿区含矿闪长岩的氧逸度为

$\Delta\text{NNO}+1.8$, 未矿化花岗闪长岩的氧逸度为 $\Delta\text{NNO}+1.2$ 。本文采用该公式计算获得包古图 III-2 岩体石英闪长岩的相对氧逸度为 $\Delta\text{NNO}+1.4 \sim \Delta\text{NNO}+2.6$ (表 1)。对比世界范围内斑岩铜矿含矿和未矿化岩体的角闪石成分发现, 含矿岩体氧逸度变化范围很大 ($\Delta\text{NNO}+0.1 \sim \Delta\text{NNO}+2.7$), 峰值集中在 $\Delta\text{NNO}+1.2 \sim \Delta\text{NNO}+1.4$ (图 7c); 未矿化岩体氧逸度变化范围较小 ($\Delta\text{NNO}+0.2 \sim \Delta\text{NNO}+2.1$), 峰值集中在 $\Delta\text{NNO}+0.8 \sim \Delta\text{NNO}+1.2$ (图 7d)。包古图 III-2 岩体分布在含矿岩体的范围内。

角闪石成分还可提供结晶温度和压力信息, 根据 Schmidt (1992) 给出的角闪石全铝压力计 ($P = -3.01 + 4.76 \text{ Al}_{\text{Tot}}$) 获得包古图 III-2 岩体角闪石的结晶压力为 $0.01 \sim 1.39 \text{ kbar}$ 。同时根据 Ridolfi et al. (2010) 提出的角闪石单矿物温度计 ($T = -151.487 \text{ Si}^* + 2041$) 获得角闪石的结晶温度为 $803 \sim 836^\circ\text{C}$ 。结合 NNO 缓冲对与温度、压力之间的关系式 (Huebner et al., 1970) 确定出岩浆体系的 $\log f_{O_2}$ 值为 $-12.37 \sim -10.69$, 投影于斑岩铜矿含矿岩体的分布范围内 (图 7b)。

6.1.2 锆石 $\text{Ce}^{4+}/\text{Ce}^{3+}$ 、 Eu/Eu^* 比值

锆石是中酸性侵入岩常见的副矿物, 其分布广泛、地球化学性质稳定, 记录了结晶时的年龄、温度、氧逸度等信息。REE 元素中的 Ce 和 Eu 是变价元素 (REE 为 REE^{3+} , Ce 可以呈现 Ce^{4+} , Eu 可以呈现 Eu^{2+}), 其价态与岩浆的氧化还原状态有关。高氧逸度状态下, 大量的 Ce^{3+} 被氧化为 Ce^{4+} , 而 Ce^{4+} 与 Zr^{4+} 离子半径相似、电价相同, 可以类质同相置换的方式进入锆石晶格。因此, 在球粒陨石标准化的稀土配分模式图上锆石显示 Ce 的正异常, 锆石的 $\text{Ce}^{4+}/\text{Ce}^{3+}$ 比值可用于指示岩浆的氧化状态。在 Ce 异常计算过程中, Ce^{3+} 通常根据相邻的 La 和 Pr 计算获得。但是, 由于锆石中这两个元素的含量很低, 接近 LA-ICP-MS 的测试极限, 通过这种方法很难准确获得 Ce^{3+} 的含量值。因此, 我们选择 Ballard et al. (2002) 给出的公式:

$$\left(\frac{\text{Ce}^{4+}}{\text{Ce}^{3+}}\right)_{\text{锆石}} = \left(\frac{\text{Ce}_{\text{熔体}} - \text{Ce}_{\text{锆石}} / D_{\text{Ce}^{3+}}^{\text{锆石/熔体}}}{\text{Ce}_{\text{锆石}} / D_{\text{Ce}^{4+}}^{\text{锆石/熔体}} - \text{Ce}_{\text{熔体}}}\right)$$

来进行锆石 Ce 异常的计算。需要注意的是, 该公式在使用过程中, $\text{Ce}_{\text{熔体}}$ 由全岩样品的 Ce 含量给出。这就意味着, 如果有富含稀土元素的矿物 (如榍石、独居石、金红石等) 先于或与锆石同时结晶, 就会对该公式的计算结果产生显著影响。Zou Xinyu

表 2 新疆包古图 III-2 岩体锆石 LA-ICP-MS 测试结果 ($\times 10^{-6}$)Table 2 LA-ICP-MS trace element data of zircons from the Baogutu intrusion III-2, Xinjiang ($\times 10^{-6}$)

测点号	09BGT-26-1	09BGT-26-3	09BGT-26-5	09BGT-26-6	09BGT-26-8	09BGT-26-11	09BGT-26-12	09BGT-26-13	09BGT-26-14	09BGT-26-15
Al	1.78	580.08	12.02	7.82	3.48	211.39	3.65	3.52	2.21	1.34
Si	153225	153225	153225	153225	153225	153225	153225	153225	153225	153225
P	308	240	213	168	256	248	297	269	274	261
Ti	10.85	18.11	8.32	8.17	8.51	28.72	8.52	9.41	10.83	9.86
Y	1333	935	1198	435	1006	979	983	1079	928	1082
Zr	408301	409601	416716	418951	419753	414501	420298	419762	417104	411367
Nb	0.67	0.30	0.47	0.27	0.31	0.63	0.63	0.47	0.61	0.50
La	bdl	0.17	bdl	bdl	bdl	0.12	bdl	bdl	bdl	bdl
Ce	10.31	6.91	8.60	4.02	6.42	8.96	8.42	7.15	7.04	8.37
Pr	0.11	0.11	0.08	0.03	0.10	0.10	0.07	0.07	0.05	0.09
Nd	2.11	1.79	1.76	0.52	1.97	1.43	1.13	1.40	1.07	1.93
Sm	4.12	3.50	4.14	1.33	4.25	2.67	2.67	3.26	2.31	4.07
Eu	1.28	0.87	1.16	0.43	1.04	0.97	0.73	1.00	0.71	0.99
Gd	23.46	19.51	21.89	7.53	20.60	14.85	16.10	18.59	13.32	20.89
Tb	8.76	6.89	8.03	2.90	7.27	5.62	6.06	7.07	5.02	7.57
Dy	109.41	82.87	99.69	35.14	88.31	71.90	77.24	88.78	67.25	92.95
Ho	43.93	31.36	39.73	14.23	33.80	30.65	31.48	35.21	29.22	36.18
Er	203	139	185	67.95	152	152	151	166	149	164
Tm	43.18	28.60	39.00	15.19	31.46	34.77	33.44	35.79	34.12	34.70
Yb	429	276	382	157	308	370	345	363	363	345
Lu	80.91	50.84	71.55	31.11	57.00	75.10	66.46	69.39	73.34	63.42
Hf	7525	8155	8354	7858	8440	7532	8354	7559	7395	7876
Ta	0.20	0.11	0.17	0.12	0.14	0.18	0.25	0.16	0.23	0.19
Th	48.97	39.14	43.76	18.74	32.41	53.70	39.74	32.89	30.10	35.72
U	79.29	54.41	69.23	40.98	52.45	84.12	79.17	59.03	72.80	60.41
REE	959	648	863	338	713	769	740	797	745	780
Eu/Eu*	0.40	0.32	0.37	0.42	0.34	0.47	0.34	0.39	0.39	0.33
Ce ⁴⁺ /Ce ³⁺	51.46	31.22	53.36	78.93	29.55	64.32	78.40	54.59	89.50	44.25
T(°C)	782	836	756	754	758	890	758	768	781	772
δK	-1.97	-0.37	-0.25	-0.18	-0.27	0.05	-0.17	-0.22	0.03	-0.24

注:锆石 Ce⁴⁺/Ce³⁺ 和 Eu_N/Eu_N^{*} 比值根据 Ballard et al. (2002) 计算; 锆石结晶温度根据 Ferry et al. (2007) 计算; 偏离系数 δK 根据 Zou et al. (2019) 计算。

et al. (2019) 给出了一个偏离系数 δK, 用于限定全岩成分对熔体成分的偏离程度。并指出, 只有 δK < 3 的锆石才能给出可信的 Ce⁴⁺/Ce³⁺ 比值。包古图 III-2 岩体锆石的 δK 值为 -1.97~0.05, 指示全岩成分可有效代表熔体成分。进一步计算获得包古图 III-2 岩体锆石的 Ce⁴⁺/Ce³⁺ 比值为 29.55~89.50。

与 Ce 异常类似, 锆石的 Eu 异常也可指示岩浆的氧化状态。在氧化条件下, 大量的 Eu²⁺ 被氧化为 Eu³⁺, Eu³⁺ 在锆石中的分配系数远大于 Eu²⁺, 锆石 Eu 含量升高, 显示弱负或无 Eu 异常。需要注意的是, 锆石的 Eu/Eu* 比值容易受到斜长石、角闪石、磷灰石等早期矿物相影响。Eu 在斜长石中的分配系数较高, 早期结晶的斜长石会强烈消耗岩浆中的 Eu, 导致锆石显示强负 Eu 异常。角闪石和磷灰石中 Eu 的分配系数较小, 二者的早期结晶会导致锆

石 Eu 负异常减弱。分析发现, III-2 岩体全岩样品 Eu/Eu* 比值中等 (0.92~1.44, 平均 1.21, Wei Shaoni, 2012), 球粒陨石标准化的稀土配分模式图上显示弱的 Eu 正异常。这说明早期结晶的矿物相对体系 Eu 异常的影响相互抵消, 锆石的 Eu/Eu* 比值可用于指示岩浆的氧化状态。根据 $Eu/Eu^* = (Eu_N / (Sm_N \times Gd_N))^{1/2}$ 计算获得包古图 III-2 岩体锆石的 Eu/Eu* 比值为 0.32~0.47。

关于锆石 Ce⁴⁺/Ce³⁺ 和 Eu/Eu* 比值对岩浆氧逸度的定量指示意义, 不同学者有不同的观点。例如, Ballard et al. (2002) 认为 Ce⁴⁺/Ce³⁺ > 300、Eu/Eu* > 0.4 是划分智利北部含矿与不含矿岩体的界线。Liang Huaying et al. (2006) 给出 Ce⁴⁺/Ce³⁺ > 120 为区分玉龙含矿和不含矿侵入体的界限值。Wang Rui et al. (2014) 认为岗底斯东部中新世成

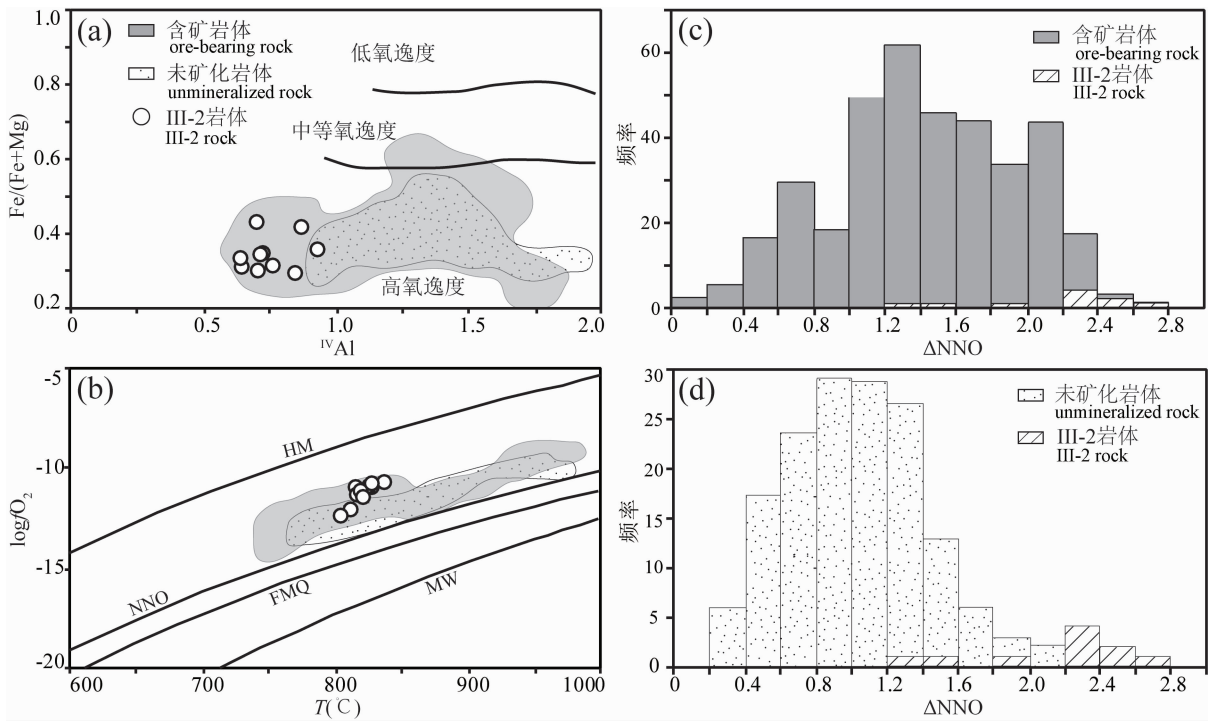


图7 新疆包古图斑岩铜矿角闪石成分及相关参数图解

Fig. 7 Plots and histograms of compositions and parameters estimated from amphiboles from porphyry copper deposits in Baogutu, Xinjiang

(a) 一角闪石 $\text{Fe}/(\text{Fe}+\text{Mg})\text{-IVAl}$ 图解(据 Anderson et al., 1995); (b) 一氧逸度-温度图解($P=1\text{kbar}$); (c) 一含矿岩体 ΔNNO 直方图; (d) 一未矿化岩体 ΔNNO 直方图. 文献数据来自 Ayati et al., 2012, Wang Rui et al., 2014, Shen Ping et al., 2015a, Sun Jia et al., 2017, Li Jinxiang et al., 2018, Wei Shaoni et al., 2019, Zarasvandi et al., 2019. HM—赤铁矿-磁铁矿缓冲对 (Spencer et al., 1981), NNO—镍-氧化镍缓冲对 (Huebner et al., 1970), FMQ—铁橄榄石-磁铁矿-石英缓冲对 (Huebner, 1971), MW—方铁矿-磁铁矿缓冲对 (Eugster et al., 1962)

(a) — $\text{Fe}/(\text{Fe}+\text{Mg})$ vs. IVAl diagram of amphibole (after Anderson et al., 1995); (b) — $\log f_{\text{O}_2}$ vs. T diagram ($P=1\text{kbar}$); (c) — ΔNNO histogram for ore-bearing intrusions; (d) — ΔNNO histogram for barren intrusions. Literature data from Ayati et al., 2012, Wang Rui et al., 2014, Shen Ping et al., 2015a, Sun Jia et al., 2017, Li Jinxiang et al., 2018, Wei Shaoni et al., 2019, Zarasvandi et al., 2019. HM—hematite-magnetite buffer (Spencer et al., 1981), NNO—nickel-nickel oxide buffer (Huebner et al., 1970), FMQ—fayalite-magnetite-quartz buffer (Huebner, 1971), MW—wustite-magnetite buffer (Eugster et al., 1962)

矿岩浆的 $\text{Ce}^{4+}/\text{Ce}^{3+} > 50$ 。我们将包古图 III-2 岩体锆石 $\text{Ce}^{4+}/\text{Ce}^{3+}$ 和 Eu/Eu^* 比值与世界范围内的典型斑岩铜矿床进行了对比(表 3, 图 8)。由对比结果可知, 含矿岩体的 $\text{Ce}^{4+}/\text{Ce}^{3+}$ 和 Eu/Eu^* 比值变化范围很大, $\text{Ce}^{4+}/\text{Ce}^{3+}$ 比值在 0~100 范围内出现明显峰值, 在 100~900 范围内连续分布, 在 100~200 和 500~700 范围内出现次级峰值(图 8a), Eu/Eu^* 比值的峰值出现在 0.6~0.7 范围内(图 8b)。不含矿岩体的 $\text{Ce}^{4+}/\text{Ce}^{3+}$ 和 Eu/Eu^* 比值分布范围较小, $\text{Ce}^{4+}/\text{Ce}^{3+}$ 比值的峰值出现在 0~100 范围内, 高 $\text{Ce}^{4+}/\text{Ce}^{3+}$ 比值(>300)的样品很少(图 8c), Eu/Eu^* 比值的峰值分布在 0.2~0.3 范围内(图 8d)。包古图 III-2 岩体锆石 $\text{Ce}^{4+}/\text{Ce}^{3+}$ (29.55~89.50) 和 Eu/Eu^* 比值(0.32~0.47)中等, 位于斑

岩铜矿含矿岩体和未矿化岩体的叠加部位(图 8e, f)。

6.2 成矿指示

斑岩矿床的形成, 是铜、金、硫等成矿组分从岩浆源区迁移至地壳浅部富集沉淀的过程, 岩浆溶解和迁移成矿组分的能力与其氧化状态密切相关。低氧逸度状态下($f_{\text{O}_2} < \text{FMQ}+2$, Mungall, 2002; Sun Weidong et al., 2015), 岩浆中的硫主要以硫化物(S^{2-})的形式存在。硫化物在岩浆中的溶解度很低, 而 Cu、Au 等亲铜元素在硫化物熔体和硅酸盐熔体间的分配系数很高($D_{\text{Cu}} = 1334 \pm 210$, Patten et al., 2013; $D_{\text{Au}} = 4500 \sim 11200$, Mungall and Brenan, 2014), 因此少量结晶的硫化物即可消耗岩浆中的大量亲铜元素。在高氧逸度状态下($f_{\text{O}_2} >$

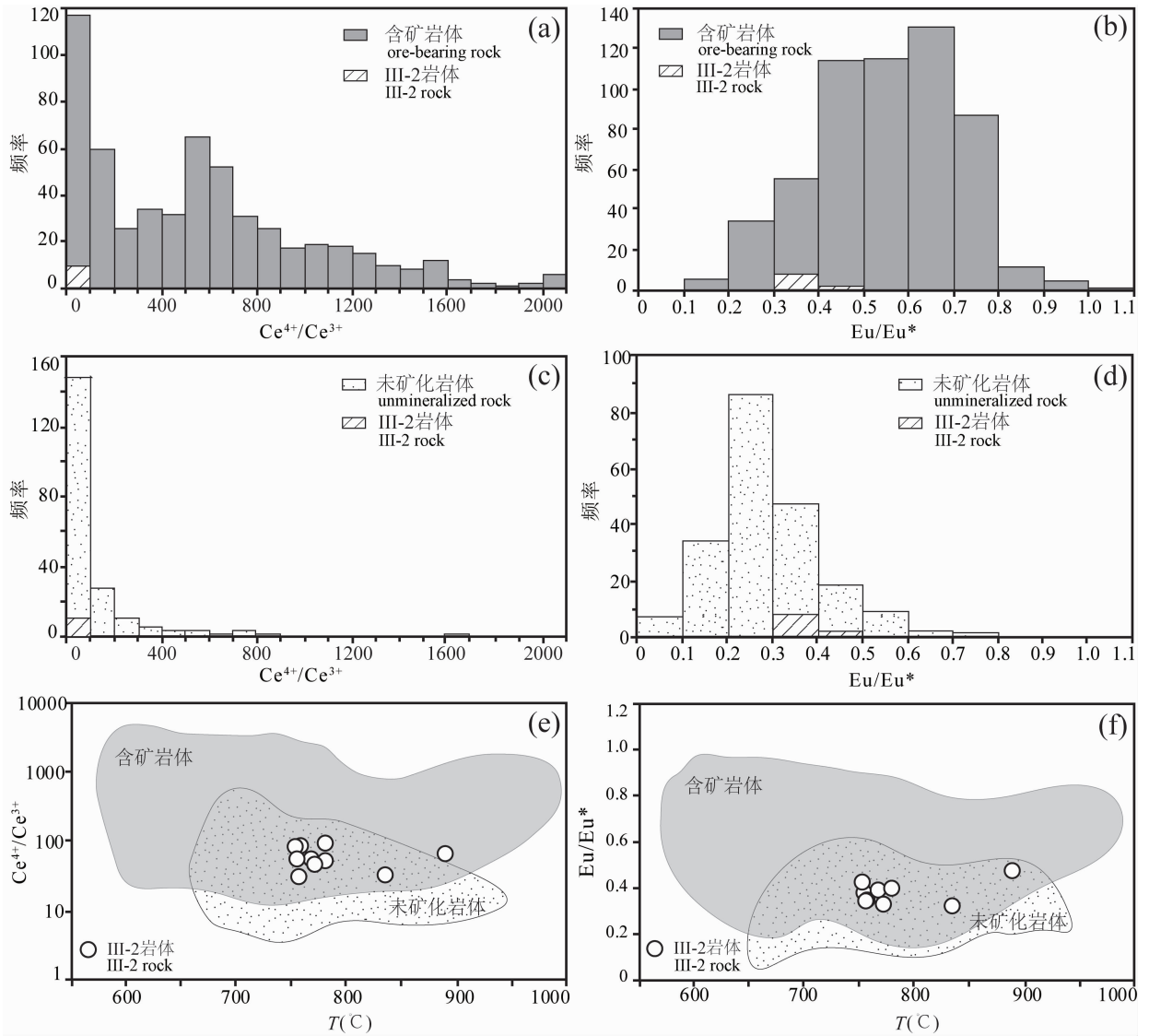


图 8 新疆包古图斑岩矿床锆石微量元素比值图解

Fig. 8 Zircon trace element ratio histograms for porphyry deposits in Baogutu, Xinjiang

(a) 含矿岩体锆石 Ce^{4+}/Ce^{3+} 比值直方图; (b) 含矿岩体锆石 Eu/Eu^* 比值直方图; (c) 未矿化岩体锆石 Ce^{4+}/Ce^{3+} 比值直方图; (d) 未矿化岩体锆石 Eu/Eu^* 比值直方图; (e) 包古图 III-2 岩体锆石 Ce^{4+}/Ce^{3+} - T 图解; (f) 包古图 III-2 岩体锆石 Eu/Eu^* - T 图解. 文献数据来源见表 3. 锆石结晶温度根据 Ferry et al. (2007) 计算
 (a)—Zircon Ce^{4+}/Ce^{3+} ratio histogram for ore-bearing intrusions; (b)—zircon Eu/Eu^* ratio histogram for ore-bearing intrusions; (c)—zircon Ce^{4+}/Ce^{3+} ratio histogram for barren intrusions; (d)—zircon Eu/Eu^* ratio histogram for barren intrusions; (e)—zircon Ce^{4+}/Ce^{3+} vs. temperature diagram for the Baogutu intrusion III-2; (f)—zircon Eu/Eu^* vs. temperature diagram for the Baogutu intrusion III-2. See table 3 for data source of the shaded region. Temperature was calculated using the Ti-inzircon thermometer based on Ferry et al. (2007)

FMQ + 2, Mungall, 2002; Sun Weidong et al., 2015), 岩浆中的硫主要以硫酸盐 (SO_4^{2-}) 的形式存在, 硫的溶解度大大增加 (高出硫化物一个数量级, Jugo et al., 2010), 同时拟制或分解早期结晶的硫化物相, 确保原始岩浆中保有丰富的 Cu、Au 含量. Shen Ping et al. (2015b) 通过对巴尔喀什-准噶尔成矿带斑岩型矿床的研究认为, 成矿岩浆的氧逸度与矿床规模之间存在正相关关系, 氧逸度越高, 矿床

规模越大. Zhang Chanchan et al. (2017) 对比了世界范围内七个典型斑岩矿床锆石 Ce^{4+}/Ce^{3+} 比值与铜储量之间的关系, 获得了相同的认识.

角闪石成分氧逸度计指示包古图 III-2 岩体的氧逸度值为: $\Delta NNO + 1.4 \sim \Delta NNO + 2.6$, 与世界范围内其他斑岩矿床角闪石数据对比发现, 包古图斑岩铜矿位于含矿岩体的氧逸度变化范围 (图 7). 同时, 包古图 III-2 岩体具有中等的锆石 Ce^{4+}/Ce^{3+}

表3 新疆包古图斑岩矿床锆石 Ce^{4+}/Ce^{3+} 和 Eu/Eu^* 比值总结Table 3 Summary of zircon Ce^{4+}/Ce^{3+} and Eu/Eu^* ratios from porphyry deposits in Baogutu, Xinjiang

含矿岩体	Ce^{4+}/Ce^{3+}	Eu/Eu^*	T(°C)	参考文献
Chuquicamata El Abar	91~2341	0.23~0.95	—	Ballard et al., 2002
El Teniente	26.8~2718	0.17~0.64	613~813	Muñoz et al., 2012
Kalmakyr	387~1621	0.16~1.02	—	Zhao Xiaobo et al., 2017
Bozshakol	77~528	0.54~0.79	683~748	Shen Ping et al., 2015b
Nurkazghan	74~362	0.43~0.61	717~792	Shen Ping et al., 2015b
Kounrad	81~592	0.43~0.57	678~766	Shen Ping et al., 2015b
Aktogai	98~248	0.41~0.60	736~806	Shen Ping et al., 2015b
Erdenet	75~256	0.27~0.33	748~812	Shen Ping et al., 2015b
Koksai	129~204	0.51~0.58	682~721	Shen Ping et al., 2015b
土屋-延东	74~332	0.28~0.40	648~693	Shen Ping et al., 2015b
Borly	29~158	0.24~0.51	719~824	Shen Ping et al., 2015b
岗底斯含矿岩浆岩	18.62~141.86	0.19~0.87	604~782	Wang Rui et al., 2014
玉龙	5~765	—	—	Liang Huaying et al., 2006
扎拉杂	26~729	—	—	Liang Huaying et al., 2006
莽总	18~1230	—	—	Liang Huaying et al., 2006
多霞松多	10~1314	—	—	Liang Huaying et al., 2006
马拉松多	17~1304	—	—	Liang Huaying et al., 2006
普朗	65~1128	0.5~0.7	649~863	Kong Dexin et al., 2016
烂泥塘	162.59~620.52	0.54~1.00	581~918	Yu Yifan et al., 2016
德兴	176~1922	0.51~0.82	588~1085	Zhang Hong et al., 2013; Zhang Chanchan et al., 2017
沙溪	186~1972	0.62~0.87	607~715	Deng Jianghong et al., 2016
罗卜岭	152~2621	0.4~0.9	610~752	Li Bin et al., 2017; Li Congying et al., 2017
包古图	15.91~163.30	0.25~0.57	657~947	Shen Ping et al., 2015b; Wei Shaoni et al., 2019; 本研究
未矿化岩体				
Chuquicamata El Abar	5~1689	0.05~0.72	—	Ballard et al., 2002
岗底斯	6.04~66.75	0.08~0.61	665~889	Wang Rui et al., 2014
沙溪	6~372	0.19~0.44	680~936	Deng Jianghong et al., 2016

(29.55~89.50) 和 Eu/Eu^* 比值 (0.32~0.47), 位于斑岩铜矿含矿岩体和未矿化岩体的叠加部位 (图8)。现有数据和对比结果显示, 包古图斑岩铜矿成矿岩浆氧逸度较高, 对成矿元素的溶解和迁移有利。

7 结论

(1) 包古图斑岩铜矿 III-2 岩体岩性均一, 以石英闪长(玢)岩和闪长岩为主。早期结晶的角闪石富 $Mg(Mg^{\#} = 0.72 \sim 1.00)$, 角闪石成分氧逸度计指示成矿岩浆的氧逸度为 $\Delta NNO + 1.4 \sim \Delta NNO + 2.6$, 位于斑岩铜矿含矿岩体的分布范围。

(2) 锆石富含稀土, 具有左倾型的稀土配分模式。锆石 Ce^{4+}/Ce^{3+} 比值为 29.55~89.50, Eu/Eu^* 比值为 0.32~0.47, 位于斑岩铜矿含矿岩体和未矿化岩体的叠加部位。

(3) 包古图斑岩铜矿 III-2 岩体成矿岩浆氧逸度较高, 有利于成矿元素的溶解和迁移。

致谢: 野外工作得到了武警黄金第八支队的支持和帮助; 中科院地质与地球物理研究所毛騫研究员、西北大学柳小明老师指导完成实验工作, 在此谨

表衷心感谢。感谢匿名审稿人的意见和建议, 对完善本文有重要意义。

References

- An Fang, Zhu Yongfeng. 2009. SHRIMP U-Pb zircon ages of tuff in Baogutu Formation and their geological significances. *Acta Petrologica Sinica*, 25: 1437~1445 (in Chinese with English abstract).
- Andersen D J, Smith D R. 1995. The effects of temperature and f_{O_2} on the Al-in-hornblende barometer. *American Mineralogist*, 80(5): 549~559.
- Ayati F, Yavuz F, Asadi H H, Richards J P, Jourdan F. 2012. Petrology and geochemistry of calc-alkaline volcanic and subvolcanic rocks, Dalli porphyry copper-gold deposit, Markazi Province, Iran. *International Geology Review*, 1: 1~27.
- Ballard J R, Palin J M, Campbell I H. 2002. Relative oxidation states of magmas inferred from $Ce(IV)/Ce(III)$ in zircon: Application to porphyry copper deposits of northern Chile. *Contributions to Mineralogy and Petrology*, 144: 347~364.
- Bao Xinchang, Yang Liqiang, He Wenyan, Gao Xue. 2018. Importance of magmatic water content and oxidation state for porphyry-style Au mineralization: An example from the giant Beiya Au deposit, SW China. *Minerals*, 8: 441~453.
- Bureau of Geology and Mineral Resources of Xinjiang. 1993. *Regional Geology of Xinjiang. Uygur Autonomous Region*. Geological Publishing House, Beijing, 1~841 (in Chinese with English abstract).
- Cao Mingjian, Qin Kezhang, Li Guangming, Evans N J, Hollings P, Maisch M, Kappler A. 2017. Mineralogical evidence for

- crystallization conditions and petrogenesis of ilmenite-series I-type granitoids at the Baogutu reduced porphyry Cu deposit (Western Junggar, NW China): Mossbauer spectroscopy, EPM and LA-(MC)-ICPMS analyses. *Ore Geology Reviews*, 86: 382~403.
- Cao Mingjian, Qin Kezhang, Li Guangming, Jin Luying, Evans N J, Yang Xiangrong. 2014. Baogutu: An example of reduced porphyry Cu deposit in western Junggar. *Ore Geology Reviews*, 56: 159~180.
- Chambefort I, Dilles J H, Kent A J R. 2008. Anhydrite-bearing andesite and dacite as a source for sulfur in magmatic-hydrothermal mineral deposits. *Geology*, 36: 719~722.
- Chen Bo, Zhu Yongfeng. 2011. Petrology, geochemistry and zircon U-Pb chronology of gabbro in Darbut ophiolitic mélange, Xinjiang. *Acta Petrologica Sinica*, 27(6): 1746~1758 (in Chinese with English abstract).
- Deng Jianghong, Yang Xiaoyong, Li Shuang, Gu Huangling, Mastoi A S, Sun Weidong. 2016. Partial melting of subducted paleo-Pacific plate during the early Cretaceous: Constraint from adakitic rocks in the Shaxi porphyry Cu-Au deposit, Lower Yangtze River Belt. *Lithos*, 262: 651~667.
- Duan Fenghao, Li Yongjun, Wang Ran, Zhi Qian, Chao Wendi, Ma Yonglin. 2018. LA-ICP-MS Zircon U-Pb geochronology and geochemical characteristics of the Tasikuola Granite in Western Junggar, Xinjiang and its geological significance. *Acta Geologica Sinica*, 92(7): 1401~1417 (in Chinese with English abstract).
- Eugster H P, Wones D R. 1962. Stability relations of the ferruginous biotite, annite. *Journal of Petrology*, 3: 82~125.
- Ferry J M, Watson E B. 2007. New thermodynamic models and revised calibrations for the Ti-in-zircon and Zr-in-rutile thermometers. *Contributions to Mineralogy and Petrology*, 154: 429~437.
- Gao Rui, Xiao Long, Pirajno F, Wang Guocan, He Xinxing, Yang Gang, Yan Shengwu. 2014. Carboniferous-Permian extensive magmatism in the West Junggar, Xinjiang, northwestern China: Its geochemistry, geochronology and petrogenesis. *Lithos*, 204: 125~143.
- Geng Hongyan, Sun Min, Yuan Chao, Xiao Wenjiao, Xian Weisheng, Zhao Guochun, Zhang Lifeng, Wong K, Wu Fuyuan. 2009. Geochemical, Sr-Nd and zircon U-Pb-Hf isotopic studies of Late Carboniferous magmatism in the West Junggar, Xinjiang: Implications for ridge subduction? *Chemical Geology*, 266: 364~389.
- Grove T L, Elkins-Tanton L T, Parman S W, Müntener O, Gaetani G A. 2003. Fractional crystallization and mantle melting controls on calc-alkaline differentiation trends. *Contributions to Mineralogy and Petrology*, 145: 515~533.
- Han Baofu, Ji Jianqing, Song Biao, Chen Lihui, Zhang Lei. 2006. Late Paleozoic vertical growth of continental crust around the Junggar Basin, Xinjiang, China (part 1): Timing of post collisional plutonism. *Acta Petrologica Sinica*, 22(5): 1077~1086 (in Chinese with English abstract).
- Han Baofu, Wang Shiguang, Jahn B M, Hong Dawei, Kagami H, Sun Yuanlin. 1997. Depleted-mantle source for the Ulungur River A-type granites from North Xinjiang, China: Geochemistry and Nd-Sr isotopic evidence, and implications for Phanerozoic crustal growth. *Chemical Geology*, 138: 135~159.
- Hattori K. 2018. Porphyry copper potential in Japan based on magmatic oxidation state. *Resource Geology*, 68(2): 126~137.
- Huebner J S, Sato M. 1970. The oxygen fugacity-temperature relationships of manganese oxide and nickel oxide buffers. *American Mineralogist*, 55: 934~952.
- Huebner J S. 1971. Buffering techniques for hydrostatic systems at elevated pressure, in Ulmer, G. C., ed., *Research techniques for high pressure and high temperature*; New York. Springer-Verlag: 123~177.
- Jugo P J, Wilke M, Botcharnikov R E. 2010. Sulfur K-edge XANES analysis of natural and synthetic basaltic glasses: Implications for S speciation and S content as function of oxygen fugacity. *Geochimica et Cosmochimica Acta*, 74: 5926~5938.
- Kong Dexin, Xu Jifeng, Chen Jianlin. 2016. Oxygen isotope and trace element geochemistry of zircons from porphyry copper system: implications for Late Triassic metallogenesis within the Yidun Terrane, southeastern Tibetan Plateau. *Chemical Geology*, 441: 148~161.
- Leake B E, Woolley A R, Birch W D. 1997. Nomenclature of Amphiboles: Report of the subcommittee on amphiboles of the international mineralogical association commission on new minerals and mineral names. *Mineralogical Magazine*, 61: 295~321.
- Li Bin, Jiang Shaoyong. 2017. Genesis of the giant Zijinshan epithermal Cu-Au and Luoboling porphyry Cu-Mo deposits in the Zijinshan ore district, Fujian Province, SE China: A multi-isotope and trace element investigation. *Ore Geology Reviews*, 88: 753~767.
- Li Congying, Hao Xiluo, Liu Jiqiang, Ling Mingxing, Ding Xing, Zhang Hong, Sun Weidong. 2017. The formation of Luoboling porphyry Cu-Mo deposit: Constraints from zircon and apatite. *Lithos*, 272-732: 291~300.
- Li Jinxiang, Qin Kezhang, Li Guangming, Evans N J, Zhao Junxing, Yue Yahui, Xie Jing. 2018. Volatile variations in magmas related to porphyry Cu-Au deposits: Insights from amphibole geochemistry, Duolong district, central Tibet. *Ore Geology Reviews*, 95: 649~662.
- Li Xinzi, Han Baofu, Ji Jianqi, Li Zonghuai, Liu Zhiqiang, Yang Bin. 2004. Geology, geochemistry and K-Ar ages of the Karamay basic-intermediate dyke swarm from Xinjiang, China. *Geochimica*, 33: 574~584 (in Chinese with English abstract).
- Liang Huaying, Campbell I H, Allen C, Sun Weidong, Liu Congqiang, Yu Hengxiang, Xie Yingwen, Zhang Yuqiang. 2006. Zircon Ce^{4+}/Ce^{3+} ratios and ages for Yulong ore-bearing porphyries in eastern Tibet. *Mineralium Deposita*, 41: 152~159.
- Liu Yulin, Guo Lishuang, Song Huixia, Song Biao, Zhang Rui, Xu Fajun, Zhang Yunxiao. 2009. Geochronology of Baogutu porphyry copper deposit in Western Junggar area, Xinjiang of China. *Science in China Series D: Earth Sciences*, 52(10): 1543~1549.
- Mungall J E, Brenan J M. 2014. Partitioning of platinum-group elements and Au between sulfide liquid and basalt and the origins of mantle-crust fractionation of the chalcophile elements. *Geochimica Cosmochimica Acta*, 125: 265~289.
- Mungall J. 2002. Roasting the mantle: slab melting and the genesis of major Au and Au-rich Cu deposits. *Geology*, 30: 915~918.
- Munoz M, Charrier R, Fanning C M, Maksav V, Deckart K. 2012. Zircon trace element and O-Hf isotope analyses of mineralized intrusions from El Teniente ore deposit, Chilean Andes: constraints on the source and magmatic evolution of porphyry Cu-Mo related magmas. *Journal of Petrology*, 53: 1091~1122.
- Patten C, Barnes S J, Mathez E A, Jenner F E. 2013. Partition coefficients of chalcophile elements between sulfide and silicate melts and the early crystallization history of sulfide liquid: LAICP-MS analysis of MORB sulfide droplets. *Chemical Geology*, 358: 170~188.
- Pichavant M, Martel C, Bourdier J L, Scaillet B. 2002. Physical conditions, structure, and dynamics of a zoned magma chamber; Mount Pelee (Martinique, Lesser Antilles Arc). *Journal of Geophysical Research*, 107(B5): ECV 1-1~ECV 1-28.
- Ren Rong, Han Baofu, Xu Zhao, Zhou Yinzhang, Liu Bo, Zhang Lei, Chen Jiafu, Su Li, Li Jiao, Li Xianhua, Li Qiuli. 2014. When did the subduction first initiate in the southern Paleo-Asian Ocean; New constraints from a Cambrian intra-oceanic arc system in West Junggar, NW China. *Earth and Planetary*

- Science Letters, 388: 222~236.
- Richards J P. 2005. Cumulative Factors in the Generation of Giant Calc-alkaline Porphyry Cu Deposits; in Porter, T. M. (Ed.), Super Porphyry Copper & Gold Deposits: A Global Perspective; PGC Publishing, Adelaide, 1: 7~25.
- Richards J. 2003. Tectono-magmatic precursors for porphyry Cu-(Mo-Au) deposit formation. *Economic Geology*, 98: 1515~1533.
- Ridolfi F, Renzulli A, Puerini M. 2010. Stability and chemical equilibrium of amphibole in calc-alkaline magmas; An overview, new thermo barometric formulations and application to subduction-related volcanoes. *Contributions to Mineralogy and Petrology*, 160: 45~66.
- Rowins S M. 2000. Reduced porphyry copper-gold deposits: A new variation on an old theme. *Geology*, 28: 491~494.
- Scaillet B, Evans B W. 1999. The 15 June 1991 eruption of Mount Pinatubo. I. Phase equilibria and pre-eruption P-T- f_{O_2} - f_{H_2} conditions of the dacite magmas. *Journal of Petrology*, 40: 381~411.
- Schmidt M W. 1992. Amphibole composition in tonalite as a function of pressure: An experimental calibration of the Al-in hornblende barometer. *Contributions to Mineralogy and Petrology*, 110: 304~310.
- Shen Ping, Hattori K, Pan Hongdi, Jackson S, Seitmuratova E. 2015b. Oxidation condition and metal fertility of granitic magmas: zircon trace-element data from porphyry Cu deposits in the Central Asian Orogenic Belt. *Economic Geology*, 110: 1861~1878.
- Shen Ping, Pan Hongdi. 2015a. Methane origin and oxygen-fugacity evolution of the Baogutu reduced porphyry Cu deposit in the West Junggar terrain, China. *Mineral Deposita*, 50(8): 967~986.
- Shen Ping, Shen Yuanchao, Liu Tiebing, Zhang Rui, Wang Jingbin, Zhang Yunxiao, Meng Lei, Wang Lijuan, Wang Jiang. 2009. Host-rocks and alteration characters of the Baogutu porphyry copper-molybdenum deposit in Xinjiang, NW China. *Acta Petrologica Sinica*, 25(4): 777~792 (in Chinese with English abstract).
- Shen Ping, Shen Yuanchao, Pan Hongdi, Li Xianhua, Dong Lianhui, Wang Jingbin, Zhu Heping, Dai Huawu, Guan Weina. 2012. Geochronology and isotope geochemistry of the Baogutu porphyry copper deposit in the West Junggar region, Xinjiang, China. *Journal of Asian Earth Sciences*, 49: 99~115.
- Sillitoe R H. 2010. Porphyry Copper Systems. *Economic Geology*, 105: 3~41.
- Sisson T W, Grove T L. 1993. Temperature and H₂O contents of low-MgO high-alumina basalts. *Contributions to Mineralogy and Petrology*, 113: 167~184.
- Smith C M, Canil D, Rowins S M, Friedman R. 2012. Reduced granitic magmas in an arc setting: The Catface porphyry Cu-Mo deposit of the Paleogene Cascade Arc. *Lithos*, 154: 361~373.
- Song Huixia, Liu Yulin, Qu Wenjun, Song Biao, Zhang Rui, Cheng Yong. 2007. Geological characters of Baogutu porphyry copper deposit in Xinjiang, NW China. *Acta Petrologica Sinica*, 23(8): 1981~1988 (in Chinese with English abstract).
- Spencer K J, Lindsley D H. 1981. A solution model for coexisting iron titanium oxides. *American Mineralogist*, 66: 1189~1201.
- Stern C R, Funk J A, Skewes M A, Arevalo A. 2007. Magmatic anhydrite in plutonic rocks at the El Teniente Cu-Mo deposit, Chile and the role of sulfur- and copper-rich magmas in its formation. *Economic Geology*, 102: 1335~1344.
- Sun Jia, Mao Jingwen, Beaudoin G, Duan Xianzhe, Yao Fojun, Ouyang H, Wu Yue, Li Yubin, Meng Xuyang. 2017. Geochronology and geochemistry of porphyritic intrusions in the Duolong porphyry and epithermal Cu-Au district, central Tibet: Implications for the genesis and exploration of porphyry copper deposits. *Ore Geology Reviews*, 80: 1004~1019.
- Sun S S, McDonough W F. 1989. Chemical and isotopic study of oceanic basalts; Implications for mantle composition and processes. Geological Society of London, Special Publication, 42: 313~345.
- Sun Weidong. 2015. Porphyry deposits and oxidized magmas. *Ore Geology Reviews*, 65: 97~131.
- Tang Gongjian, Wang Qiang, Wyman D, Li Zhengxiang, Xu Yigang, Zhao Zhenhua. 2012. Recycling oceanic crust for continental crustal growth: Sr-Nd-Hf isotope evidence from granulites in the western Junggar region, NW China. *Lithos*, 128~131: 73~83.
- Wang Rui, Richards J P, Hou Zengqian, Yang Zhiming, Gou Zhengbin, Dufrane S A. 2014. Increasing magmatic oxidation state from paleocene to miocene in the eastern Gangdese belt, Tibet; implication for collision-related porphyry Cu-Mo ± Au mineralization. *Economic Geology*, 109(7): 1943~1965.
- Wang Rui, Tafti R, Hou Zengqian, Shen Zhichao, Guo Na, Evans N J, Jeon H, Li Qiuyun, Li Weikai. 2017. Across-arc geochemical variation in the Jurassic magmatic zone, Southern Tibet; Implication for continental arc-related porphyry Cu-Au mineralization. *Chemical Geology*, 451: 116~134.
- Wang Rui, Zhu Yongfeng. 2007. Geology of the Baobei gold deposit in western Junggar and zircon SHRIMP age of its wall-rocks, western Junggar (Xinjiang, NW China). *Geological Journal of China University*, 13(3): 590~602 (in Chinese with English abstract).
- Wei Shaoni, Zhu Yongfeng, Jiang Jiuyang, Feng Wanyi. 2019. Magmatic oxidation state of the Baogutu porphyry copper deposit in the west Junggar of China; Implication for ore-formation. *Ore Geology Reviews*, 106: 351~368.
- Wei Shaoni, Zhu Yongfeng, Zheng Bo. 2017. Characteristics of antimony mineralization in the Baogutu intrusive body III-2, Xinjiang Province. *Journal of Lanzhou University: Natural Science*, 53(5): 569~575 (in Chinese with English abstract).
- Wei Shaoni, Zhu Yongfeng. 2015. Petrology, geochronology and geochemistry of intermediate-acid intrusions in Baogutu area, west Junggar, Xinjiang. *Acta Petrologica Sinica*, 31(1): 143~160 (in Chinese with English abstract).
- Wei Shaoni. 2012. Copper-gold mineralization related to intermediate-acid intrusions in Baogutu area, west Junggar, Xinjing. Ph. D thesis of Peking University (in Chinese with English abstract).
- Williamson B J, Herrington R J, Morris A. 2016. Porphyry copper enrichment linked to excess aluminium in plagioclase. *Nature Geoscience*, 9: 237~241.
- Xu Yixian, Yang Bo, Zhang Sheng, Liu Ying, Zhu Lupei, Huang Rong, Chen Chao, Li Yongtao, Luo Yinhe. 2016. Magnetotelluric imaging of a fossil Paleozoic intra-oceanic subduction zone in western Junggar, NW China. *Journal of Geophysical Research: Solid Earth*, 121: 4103~4117.
- Yang Gaoxue, Li Yongjun, Gu Pingyang, Yang Baokai, Tong Lili, Zhang Hongwei. 2012. Geochronological and geochemical study of the Darbut Ophiolitic Complex in the West Junggar (NW China): Implications for petrogenesis and tectonic evolution. *Gondwana Research*, 21: 1037~1049.
- Yin Jiyuan, Long Xiaoping, Yuan Chao, Sun Min, Zhao Guochun, Geng Hongyan. 2013. A Late Carboniferous-Early Permian slab window in the West Junggar of NW China; Geochronological and geochemical evidence from mafic to intermediate dikes. *Lithos*, 175~176: 146~162.
- Yu Yifan, Fei Guangchun, Li Youguo, Long Xunrong, Tian Enyuan, Liu Guoqing, Lü Fengming, Hua Keqiang. 2016. Oxygen fugacity of intrusions from Lannitang porphyry copper deposit in Zhongdian island arc, Yunnan; Implications for mineralization. *Journal of Mineralogy and Petrology*, (1): 28~36 (in Chinese with English abstract).
- Zarasvandi A, Heidari M, Raith J, Rezaei M, Saki A. 2019. Geochemical characteristics of collisional and pre-collisional porphyry copper systems in Kerman Cenozoic Magmatic Arc, Iran; Using plagioclase, biotite and amphibole chemistry.

- Lithos, 326~327; 279~297.
- Zhang Chanchan, Sun Weidong, Wang Jintuan, Zhang Lipeng, Sun Saijun, Wu Kai. 2017. Oxygen fugacity and porphyry mineralization: A zircon perspective of Dexing porphyry Cu deposit, China. *Geochimica Cosmochimica Acta*, 206: 343~363.
- Zhang Hong, Ling Mingxing, Liu Yulong, Tu Xianglin, Wang Fangyue, Li Congying, Liang Huaying, Yang Xiaoyong, Arndt N T, Sun Weidong. 2013. High Oxygen Fugacity and Slab Melting Linked to Cu Mineralization: Evidence from Dexing Porphyry Copper Deposits, Southeastern China. *The Journal of Geology*, 121(3):289~305.
- Zhang Huichao, Zhu Yongfeng. 2018. Geochronology and geochemistry of the Huilvshan gabbro in west Junggar (NW China): Implications for magma process and tectonic regime. *Mineralogy and Petrology*, 112(3): 297~315.
- Zhang Jien, Xiao Wenjiao, Han Chunming, Mao Qigui, Ao Songjian, Guo Qianqian, Ma Chong. 2011. A Devonian to Carboniferous intra-oceanic subduction system in Western Junggar, NW China. *Lithos*, 125: 592~606.
- Zhang Lianchang, Wan Bo, Jiao Xuejun, Zhang Rui. 2006. Characteristics and geological significance of adakitic rocks in copper-bearing porphyry in Baogutu, Western Junggar. *Geology in China*, 33(3): 626~631 (in Chinese with English abstract).
- Zhang Rui, Zhang Yunxiao, Tong Gengsheng, Wang Jiang, Li Longqian. 2006. Major breakthrough in copper exploration in the Baogutu porphyry copper deposit, western Junggar, Xinjiang, and its significance. *Geology in China*, 33(6): 1354~1360 (in Chinese with English abstract).
- Zhao Xiaobo, Xue Chunji, Chi Guoxiang, Mo Xuanxue, Nurtaev B, Zhang Guozhen. 2017. Zircon and molybdenite geochronology and geochemistry of the Kalmayr porphyry Cu-Au deposit, Almalyk district, Uzbekistan: Implications for mineralization processes. *Ore Geology Reviews*, 86: 807~824.
- Zheng Bo, Zhu Yongfeng, An Fang, Huang Qiuyue, Qiu Tian. 2015. As-Sb-Bi-Au mineralization in the Baogutu gold deposit, Xinjiang, NW China. *Ore Geology Reviews*, 69: 17~32.
- Zhu Bin, Zhang Hongfu, Shen Ping, Su Benxun, Xiao Yan, He Yongsheng. 2018. Redox state of the Baogutu reduced porphyry Cu deposit in the Central Asian Orogenic belt. *Ore Geology Reviews*, 101: 803~818.
- Zhu Yongfeng, An Fang, Feng Wanyi, Zhang Huichao. 2016. Geological evolution and huge ore-forming belts in the core part of the central Asian Metallogenic Region. *Journal of Earth Science*, 27(3): 491~506.
- Zhu Yongfeng, Chen Bo, Qiu Tian. 2015. Geology and geochemistry of the Baijiantan-Baikougan ophiolitic mélanges: implications for geological evolution of west Junggar, Xinjiang, NW China. *Geological Magazine*, 152: 41~69.
- Zhu Yongfeng, Chen Bo, Xu Xin, Qiu Tian, An Fang. 2013. A new geological map of the western Junggar, north Xinjiang (NW China): implications for Paleoenvironmental reconstruction. *Episodes*, 36: 205~220.
- Zou Xinyu, Qin Kezhang, Han Xinlei, Li Guangming, Evans N J, Li Zhenzhen, Yang Wei. 2019. Insight into zircon REE oxybarometers: A Lattice strain model perspective. *Earth and Planetary Science Letters*, 506: 87~96.

参 考 文 献

- 安芳, 朱永峰. 2009. 新疆西准噶尔包古图组凝灰岩锆石 SHRIMP 年龄及其地质意义. *岩石学报*, 25: 1437~1445.
- 陈博, 朱永峰. 2011. 新疆达拉布特蛇绿混杂岩中辉长岩岩石学、微量元素地球化学和锆石 U-Pb 年代学研究. *岩石学报*, 27(6): 1746~1758.
- 段丰浩, 李永军, 王冉, 支倩, 晁文迪, 马勇林. 2018. 新疆西准噶尔塔斯阔腊岩体 LA-ICP-MS 锆石 U-Pb 年代学、地球化学特征及地质意义. *地质学报*, 92(7): 1401~1417.
- 韩宝福, 季建清, 宋彪, 陈立辉, 张磊. 2006. 新疆准噶尔晚古生代陆壳垂向生长(I)-后碰撞深成岩浆活动的时限. *岩石学报*, 22(5): 1077~1086.
- 李辛子, 韩宝福, 季建清, 李宗怀, 刘志强, 杨斌. 2004. 新疆克拉玛依中基性岩墙群的地质地球化学和 K-Ar 年代学. *地球化学*, 33: 574~584.
- 申萍, 沈远超, 刘铁兵, 张锐, 王京彬, 张云孝, 孟磊, 王丽娟, 汪疆. 2009. 新疆包古图斑岩型铜钼矿床容矿岩石及蚀变特征. *岩石学报*, 25(4): 777~792.
- 宋会侠, 刘玉琳, 屈文俊, 宋彪, 张锐, 成勇. 2007. 新疆包古图斑岩铜矿床地质特征. *岩石学报*, 23(8): 1981~1988.
- 王瑞, 朱永峰. 2007. 西准噶尔宝贝金矿地质与容矿火山岩的锆石 SHRIMP 年龄. *高校地质学报*, 13(3): 590~602.
- 魏少妮, 朱永峰, 郑波. 2017. 新疆包古图 III-2 号岩体梯矿化特征. *兰州大学学报: 自然科学版*, 53(5): 569~575.
- 魏少妮, 朱永峰. 2015. 新疆西准噶尔包古图地区中酸性侵入体的岩石学、年代学和地球化学研究. *岩石学报*, 31(1): 143~160.
- 魏少妮. 2012. 新疆西准噶尔包古图地区与中酸性侵入体有关的铜-金成矿作用研究. 北京大学博士研究生学位论文.
- 新疆维吾尔自治区地质矿产局. 1993. 新疆维吾尔自治区区域地质志. 北京: 地质出版社, 1~841.
- 俞一凡, 费光春, 李佑国, 龙训荣, 田恩源, 刘国庆, 吕峰明, 华柯强. 2016. 云南中甸岛弧烂泥塘斑岩铜矿床岩体氧逸度特征及成矿意义. *矿物岩石*, (1): 28~36.
- 张连昌, 万博, 焦学军, 张锐. 2006. 西准包古图含铜斑岩的埃达克岩特征及其地质意义. *中国地质*, 33(3): 626~631.
- 张锐, 张云孝, 佟更生, 汪疆, 李龙乾. 2006. 新疆西准包古图地区斑岩铜矿找矿的重大突破及意义. *中国地质*, 33(6): 1354~1360.

Oxygen fugacity of the intrusion III-2 in the Baogutu porphyry copper deposit, Xinjiang: evidence from mineral compositions

WEI Shaoni^{*1)}, ZHU Yongfeng²⁾, AN Fang³⁾

1) College of Geology and Environment, Xi'an University of Science and Technology, Xi'an, 710054;

2) School of Earth and Space Sciences, Peking University, Beijing, 100871;

3) Department of Geology, Northwest University, Xi'an, 710069

* Corresponding author: weishaoni03@163.com

Abstract

Baogutu porphyry copper deposit, the largest porphyry type deposit of the area, is located in the west Junngar, Xinjiang. The ore-forming processes are closely associated with the late Carboniferous intermediate-acidic intrusions. The intrusion III-2, located in the south of the mine, with the characteristics of wholly mineralized and low grade, is an ideal sample for investigation of the nature of the ore-forming magma. In this paper, oxygen fugacity of ore-forming magma was discussed on the basis of petrology and mineral compositions of amphibole and zircon, by comparison with typical porphyry copper deposits. The results show that the Baogutu intrusion III-2 is mainly composed of quartz diorite (porphyry) and diorite, with a small amount of pyroxene diorite. Plagioclase, amphibole, biotite, quartz and potassium feldspar are the major ore-forming minerals, with minor ilmenite, sphene and apatite. Early stage euhedral amphiboles from quartz diorite are classified as calcic amphibole with high $Mg^{\#}$ (0.72~1.00). The oxygen barometer based on amphibole compositions provides $\log f_{O_2}$ values ranging from $\Delta NNO+1.4$ to $\Delta NNO+2.6$, which is in the variation range of ore-bearing intrusions from porphyry copper deposits worldwide. Zircons from quartz diorite are characterized by high REE content ($338 \times 10^{-6} \sim 959 \times 10^{-6}$). With depleted LREE and enriched HREE, these zircons display left-leaning REE patterns and strongly positive Ce and negative Eu anomalies. The moderate Ce^{4+}/Ce^{3+} (29.55~89.50) and Eu/Eu^* ratios (0.32~0.47) are in the overlapping portion of ore-bearing and ore-barren intrusions from porphyry copper deposits. These data indicate that the oxygen fugacity of the ore-forming magma of the Baogutu intrusion III-2 are relatively high, which is beneficial for the dissolution and migration of metal elements, and also facilitates the formation of porphyry copper deposits.

Key words: oxygen fugacity; porphyry copper deposit; ore-forming magma; Baogutu; West Junngar